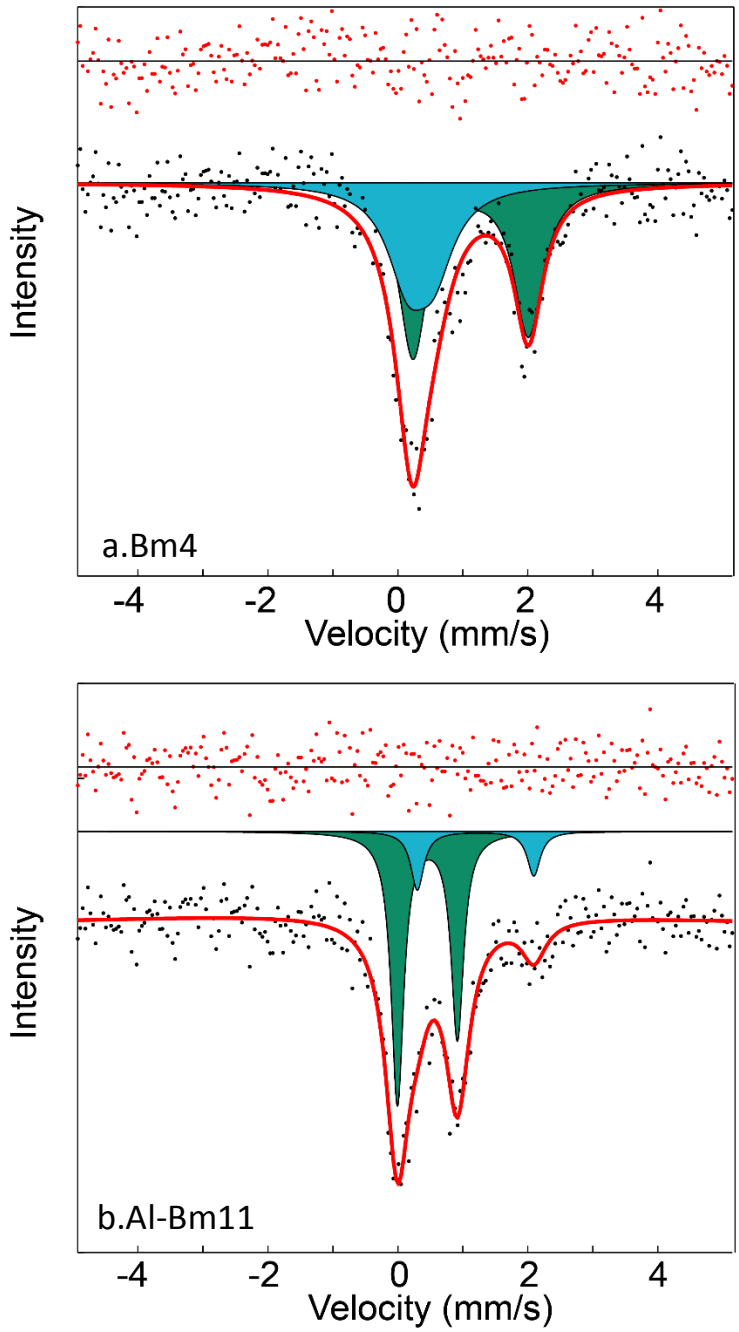

Figure S1. Convention Mössbauer spectra of Bm6 (a) and Al-Bm11 (b) at ambient conditions.

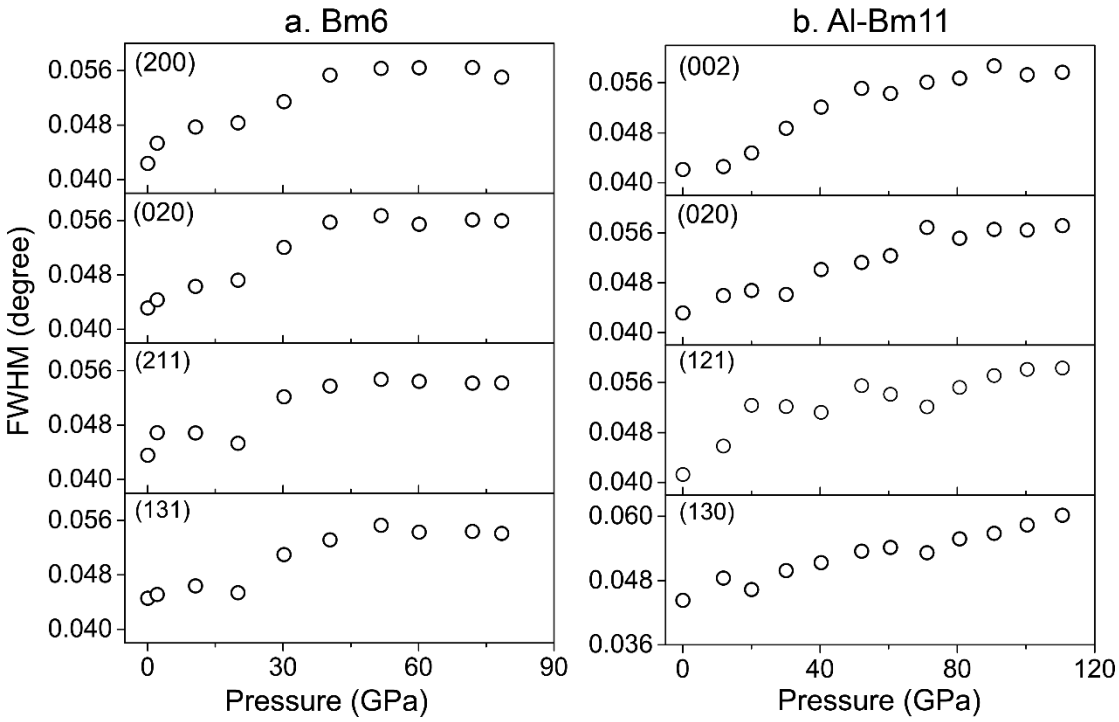

Figure S2. FWHM of selected diffraction peaks of bridgmanite single crystals with increasing pressure. (a). Bm6; (b). Al-Bm11.

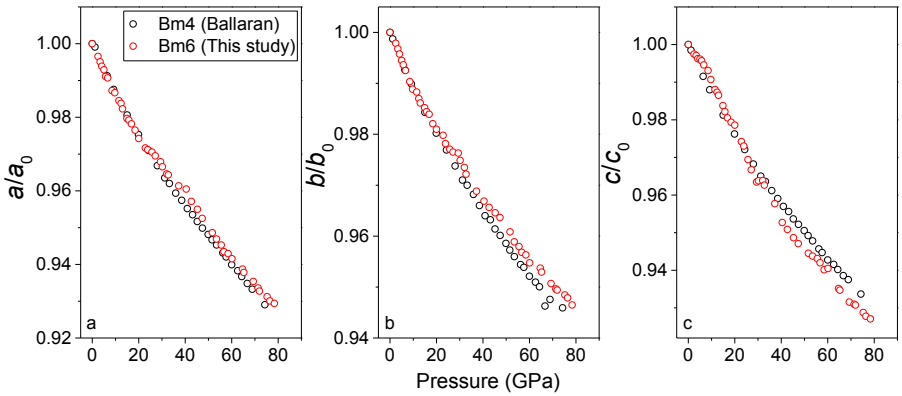

Figure S3. Comparison of the axial compression in a/a_0 (a), b/b_0 (b), and c/c_0 (c) between Bm4 (Boffa Ballaran et al. 2012) and Bm6 (this study).

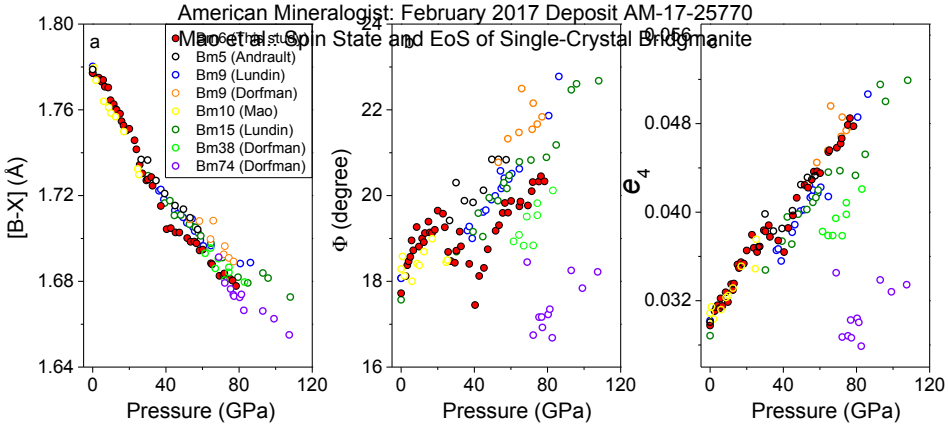

Figure S4. Octahedral bond length ([*B*-*X*]), octahedral tilting angles (ϕ), and Shear strain component (e_4) of Fe-bearing bridgmanite at high pressures and 300 K. (a). octahedral bond length, [*B*-*X*]; (b). octahedral tilting angles, ϕ; (c). shear strain component, e_4. Red: Bm6 (this study); black: Bm5 (Andrault et al. 2001); blue and olive: Bm9 and Bm15, respectively (Lundin et al. 2008); orange: Bm9, Bm38, and Bm74, respectively (Dorfman et al. 2013); yellow: Bm10 (Mao et al. 1991).

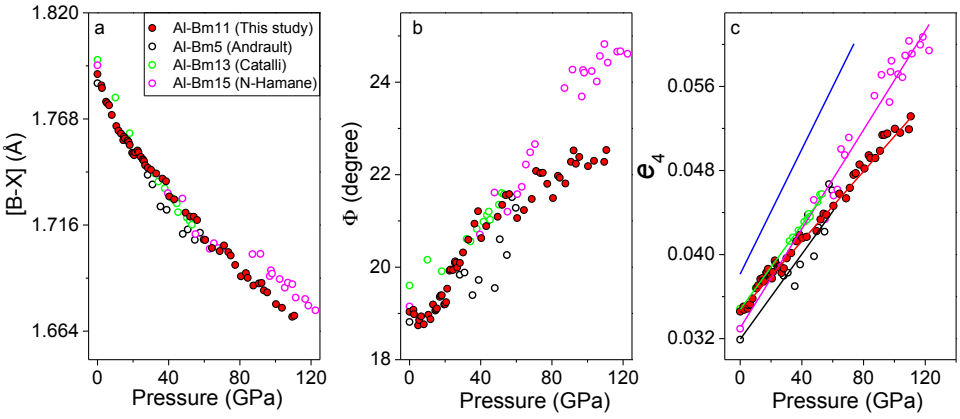

Figure S5. Octahedral bond length ([*B*-*X*]), octahedral tilting angles (ϕ), and Shear strain component (e_4) of Al-bearing bridgmanite at high pressures and 300 K. (a). octahedral bond length, [*B*-*X*]; (b). octahedral tilting angles, ϕ; (c). shear strain component, e_4. Red: Al-Bm11 (this study); black: Al-Bm5 (Andrault et al. 2001); green: Al-Bm13 (Catalli et al. 2011); magenta: Al-Bm15 (Nishio-Hamane et al. 2008).

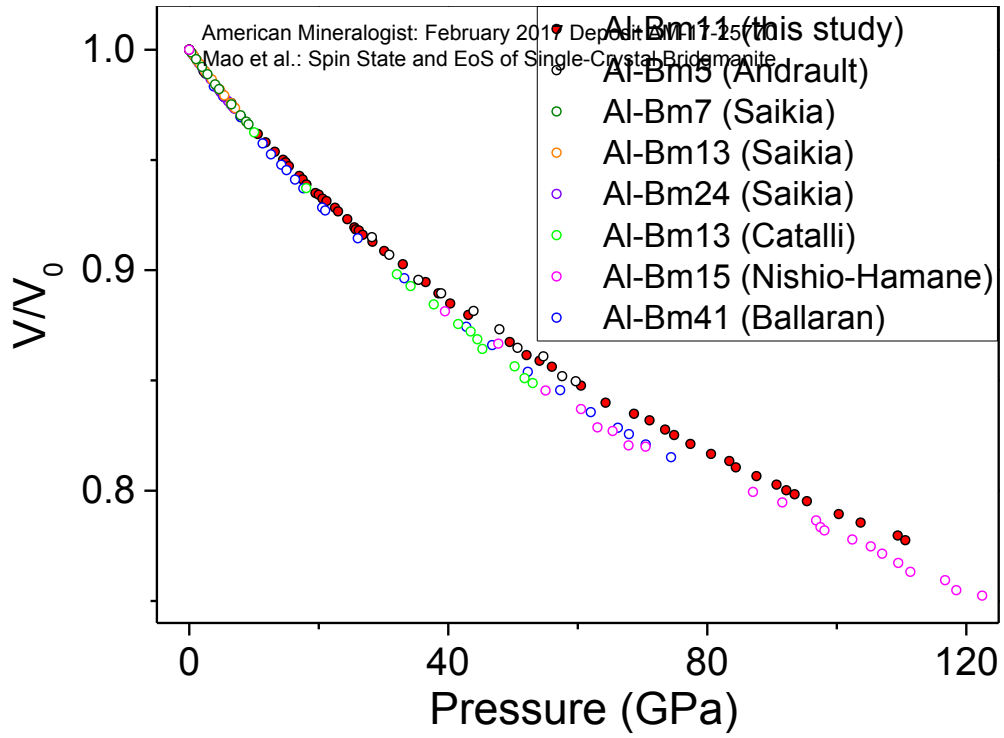

Figure S6. V/V_0 ratio of Al-bearing bridgmanite. Red: Al-Bm11 (this study); black: Al-Bm5 (Andrault et al. 2001); olive: Al-Bm7 (Saikia et al. 2009); orange: Al-Bm13 (Saikia et al. 2009); purple: Al-Bm24 (Saikia et al. 2009); green: Al-Bm13 (Catalli et al. 2011); magenta: Al-Bm15 (Nishio-Hamane et al. 2009); blue: Al-Bm41 (Boffa Ballaran et al. 2012)